Service Pressure Regulation in Water Distribution Networks

Giacomo Galuppini [a,*], Enrico Creaco[a], Chiara Toffanin[b], Lalo Magni[a]

[a]*Dipartimento di Ingegneria Civile e Architettura, University of Pavia, Pavia 27100, Italy*
[b]*Dipartimento di Ingegneria Industriale e dell'Informazione, University of Pavia, Pavia 27100, Italy*

Abstract

Real time pressure control is commonly adopted in water distribution network management to reduce leakage. A numerical description of the dynamic behaviour of the water distribution network (WDN) is introduced, allowing simulations of different case studies. A local, linear model is then identified from simulated experiments in order to synthesise different control algorithms working with control time step of 1 s. A state-of-the-art control algorithm operating with control time step of some minutes is used as benchmark. Results prove that all the new controllers reduce the control error, suggesting that cost and communication overheads introduced by control time step reduction are well motivated by sensible benefits in terms of pressure regulation.

Keywords: WDN, RTC, LQG, pressure, PCV.

1. Introduction

Due to its benefits in terms of leakage reduction [1], pipe burst abatement [2],[3] and infrastructure life extension, pressure control has recently been widely adopted in the management of water distribution networks (WDNs). After a WDN has been divided into zones of homogeneous elevation (pressure zones) for facilitating pressure regulation [4], local and remote real time control (RTC) can be adopted to drive a control valve installed in each pressure zone. The difference between local and remote RTC lies in the source of the measurements used for service pressure regulation. Local RTC is carried out by controlling a variable at the valve site (i.e. the pressure head at the valve outlet) [5],[6],[7],[8]. Remote RTC, instead, is carried out by taking as controlled variable the pressure head at the critical node, i.e. the node with minimum average pressure [9],[10],[11],[12],[13]. While being more burdensome in terms of installation costs, remote RTC is often more cost-effective in the long run [13]. In fact, it enables service pressure regulation to meet WDN demand variations in time. RTC controllers can serve as low-level controllers in hierarchical control schemes, where a high-level optimal control strategy defines the pressure setpoints for the different pressure zones, according to an economic cost-benefit evaluation over the whole network [14],[15],[16],[17],[18],[19],[20]. The operation of remote RTC can be summarized as follows. At each control time step, the pressure head is measured at the remotely controlled node. By making use of suitable algorithms operating on the pressure head measurements, a programmable logic controller sets the new suitable device setting to obtain the desired pressure at the remote node. In the works of Campisano et al. [9],[10],[11], simple proportional algorithms were used for valve control. Based on physical considerations on the WDN, Creaco and Franchini [12] developed a more effective algorithm that also makes use of the water discharge measurement in the pipe equipped with the control device. Finally, Creaco [21] and Page et al. [22] showed that implementing water discharge prediction inside the control algorithm of Creaco and Franchini [12] may be beneficial in terms of error on the controlled variable with respect to the set point and of total variations of the device setting. The benefits stand out above all when the random fluctuations of demand are insignificant compared to its hourly variations [21]. The algorithms by Campisano et al. [9],[10],[11], Creaco and Franchini [12], Creaco [21] and Page et al. [22] were all developed considering sufficiently large control time steps, e.g. order of magnitude of some minutes, across which WDN behaviour can be approximated as a sequence of steady states. The aim of this work is instead investigating the possibility of improving the regulation preformance by reducing the sampling time of the control system (down to 1 second). This requires taking into account the dynamic behaviour of the WDN. The authors tune different model-based algorithms (Proportional-Integral and Linear Quadratic Gaussian Controllers) and evaluate their performance with simulations in two different case studies. The algorithm by Creaco and Franchini [12] is used as benchmark for comparison. The following sections are associated to the description of the two case studies, together with the mathematical models of the WDN behaviour, which are used for simulations. Then the control algorithms are introduced and the tuning process described in detail. An extensive comparison of results is reported in the final section of this work.

2. Case studies

The RTC algorithms developed in this work are tested with two different WDN topologies. In both cases, nodal demands

*Corresponding author.
E-mail address: giacomo.galuppini01@ateneopv.it
Conflict of interest - none declared

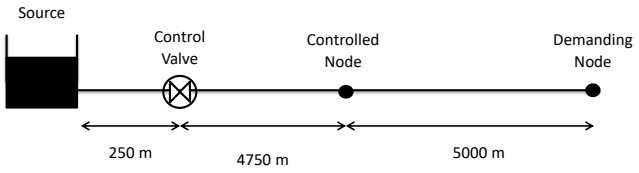

Figure 1: Case Study A: topology of the water distribution system.

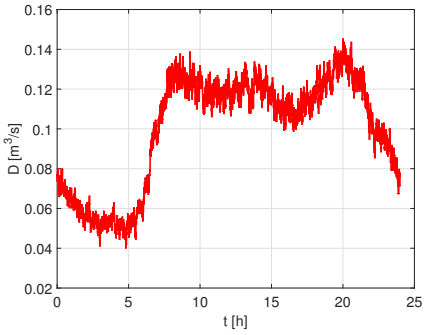

Figure 2: Case Study A: demand profile.

are generated at the temporal scale of 1 s, making use of statistic models for demand pulse generation [23]. All the proposed demand profiles follow patterns that keep into account human daily routine. Three main peaks can be identified in the daily profiles: one in the morning, one close to midday and an evening one, while demand is typically lower during night time. The profile would be flatter during day time in presence of industrial activities, whose demand is more uniform during working hours.

Case Study A, which is depicted in Figure 1, is represented by a simple water distribution system, with a tank acting as a source node and a pipe connecting it to a single demanding node. The tank provides a constant pressure of 50 m. The time behaviour of the demand is depicted in Figure 2. No leakage is considered in this system. A pressure control valve (PCV) is installed 250 m downstream the source node. The valve closure speed was set to obtain the full valve closure from the completely open position in 100 s. For control purposes, pressure is measured in the middle of the pipe. The control goal is regulation of the pressure in the middle of the pipe at $h_{sp} = 29\ m$. To test the robustness of regulation, simulations are repeated introducing different offsets in the demand profile. The offsets range in the interval $[-0.03; 0.05]$ $[m^3/s]$ and take into account seasonal variations of the demand. For Case Study A, a 2 hour simulation is also performed to evaluate the behaviour of the controller in presence of a step variation ($+ 0.03$ $[m^3/s]$) of the demand, to simulate the opening of a fire hydrant or a sudden break in the pipe.

Case Study B is represented by the skeletonized WDN of a town with about 30,000 inhabitants in Northern Italy. The network is made up of 27 nodes (26 nodes with unknown head with

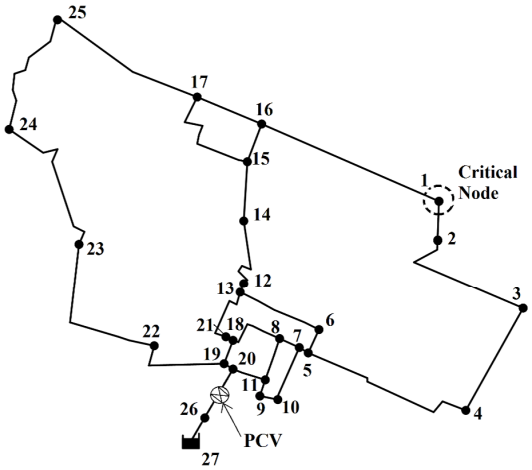

Figure 3: Case Study B: topology of the WDN

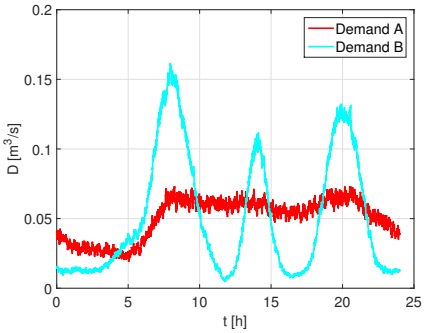

Figure 4: Case Study B: demand profiles.

ground elevation of 0 m a.s.l. and 1 source node with ground level of 35 m a.s.l.) and 32 pipes. The complete topology is depicted in Figure 3. In this case study, two demand patterns are considered [21], leading to two different trends of the total WDN demand (see Figure 4): a flatter trend (profile A) and a more peaked trend (profile B). This is done to analyse robustness of RTC with respect to different nodal demand behaviours. The source pressure head profile is instead reported in Figure 5. Other features of network nodes and pipes are reported in [23]. A PCV with diameter of 250 mm is installed in pipe 26-20 linking the source to the rest of the network. In the RTC, the critical node 1 is chosen as controlled node. The pressure set point value for the critical node is $h_{sp} = 25\ m$. The valve moves from a completely open to a completely closed position in 300 s.

The two case studies represent processes with different dynamic behaviours. The dynamics of Case Study A is in fact mainly determined by the water hammer effect, whose impact on RTC is not completely clear, in particular when the control algorithm is implemented with short sampling times (instability events that arouse in real plants have been studied in similar situations in [24] and [25]). On the other hand, the dynamic behaviour of Case Study B is given by its complex topology, while the water hammer effect is expected to play a minor role.

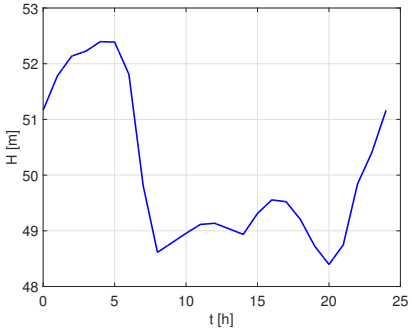

Figure 5: Case Study B: source pressure head profile.

3. Numerical model

The WDN behaviour is described by means of unsteady flow modelling [23]. This enables proper analysis of the hydraulic transients due to rapid nodal demand and/or valve setting variations.
Consider a generic pipe of a WDN. The one-dimensional unsteady flow equations take the form:

$$\begin{aligned} \frac{\partial h_p}{\partial x} + \frac{1}{gA}\frac{\partial Q}{\partial t} + J = 0 \\ \frac{\partial h_p}{\partial t} + \frac{c^2}{gA}\frac{\partial Q}{\partial x} + \frac{c^2 q}{gA} = 0 \end{aligned} \tag{1}$$

where h_p $[m]$ and Q $[m^3/s]$ are the pressure head and the flow discharge along the pipe, x $[m]$ is the position along the pipe, t $[s]$ is time, A $[m^2]$ is the pipe cross-section area, g $[m/s^2]$ is the gravity acceleration constant, c $[m/s]$ is the wave celerity, q $[m^2/s]$ is the leakage outflow per unit length, J is the friction slope.

Remark: in hydraulic framework, pressure is typically measured in $[m]$. It holds $1\ m = 9806.38\ [Pa]$, that is the pressure exercised by a one meter column of water.

The wave celerity c can be computed as:

$$c = \left(\frac{\frac{\epsilon}{\zeta}}{1 + \frac{\epsilon d}{Es}} \right)^{\frac{1}{2}} \tag{2}$$

where ϵ $[Pa]$ and ζ $[kg/m^3]$ are water bulk modulus and density; E $[Pa]$, d $[m]$ and s $[m]$ are pipe modulus of elasticity, diameter and thickness.
To account for leakage from WDN pipes, the following outflow q is considered:

$$q = \alpha_{leak} h_p^{\gamma} \tag{3}$$

where α_{leak} $[m/s]$ and γ $[-]$ are the leakage coefficient and exponent, respectively. As for leakage evaluation, exponent γ is set to 1, typical value for plastic pipes [26]. Coefficient α_{leak} $[-]$ is set to 0 and $9.4\ 10^{-9} m/s$ to obtain a leakage percentage rate of 0% and 20%, in the two case studies, respectively.
The pipe friction slope can be evaluated as:

$$J = 10.29 \frac{n^2 |Q| Q}{d^{5.33}} \tag{4}$$

where n $[s/m^{\frac{1}{3}}]$ is the Gauckler–Manning coefficient. Pipe friction slopes are then increased using the correction proposed by Pezzinga in [27], to account for the unsteady flow effects.

In the model implementation, the network pipes are discretised with spatial steps Δx. The solution of the water hammer partial differential equations through the method of the characteristics [28] enables calculating the hydraulic variables of interest (pressure and water flow) along the pipes at each time integration step Δt, with Δx and Δt such that:

$$\frac{\Delta x}{\Delta t} = c \tag{5}$$

Suitable boundary conditions are assigned in correspondence to source and demanding nodes, where fixed total pressure head and demands are prescribed, respectively. The continuity equation is introduced as well, i.e. the sum of the water discharges entering the generic demanding node through the connected pipes equals the nodal outflow, at each time integration step.

The instantaneous demand at each WDN node is evaluated using the stochastic bottom-up approach proposed in [23]. The outflow to the nodal users is evaluated by multiplying the instantaneous demand by the correction factor proposed in [29], to account from the dependence of nodal outflow on service pressure. This factor is a function of the ratio of the instantaneous pressure head h to the desired pressure head h_{sp} and ranges from 0 to 1.

The effect of the control valve is modelled by considering no link at the valve site and setting nodal inflow at the upstream end at:

$$Q_{up} = -\sqrt{\frac{2g}{\xi(\alpha)}} A \sqrt{\Delta H_{valve}} \tag{6}$$

and the inflow at the downstream end is set, instead, to:

$$Q_{down} = -Q_{up} \tag{7}$$

where ξ is the valve head loss coefficient, ΔH_{valve} is the head drop in the valve and α is the valve closure setting, ranging from 0 (fully open) to 1 (fully closed). The valve head loss coefficient is a growing function of α. This function is typically made available by the valve manufacturer.

4. Performance metrics

To quantify and compare the performances of the different control schemes, three metrics are introduced. All signals are sampled with a 1 s sampling time. Let k be the current discrete-time instant. Let $h(k)$ be the measured pressure, h_{sp} be the pressure setpoint, $\alpha(k)$ be the valve closure and $\Delta\alpha(k) = \alpha(k) - \alpha(k-1)$ be the variation of the valve closure over a single sampling time. Let $e(k) = h(k) - h_{sp}$ be the error of the controlled pressure head at time instant k. Then the metrics can be defined as follows:

- $Mean|e(k)|$ $[m]$. The *regulation error*, which evaluates the proximity of the pressure to the desired setpoint.

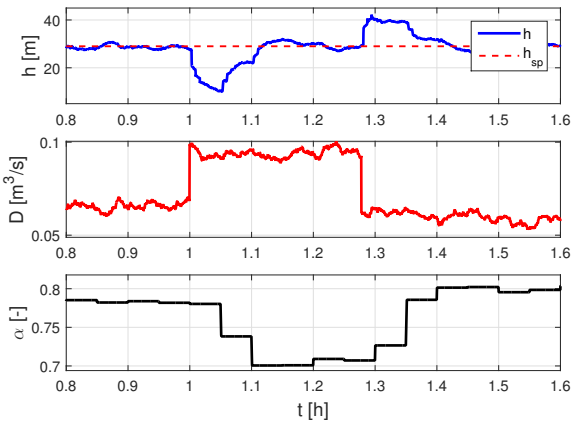

Figure 6: Case Study A: closed-loop simulation with *P on ξ* algorithm and opening of a fire hydrant. Top: pressure $h(t)$ and pressure setpoint h_{sp}. Middle: demand $D(t)$. Bottom: valve closure $\alpha(t)$.

- $\sum |\Delta\alpha(k)|$ $[-]$. The *cost of control*, which impacts on the energy required to perform regulation and on wear of actuators.
- *% of Displacement Instants* $[-]$, measuring valve activity in terms of percentage of time instants during which the actuator is in motion.

5. State of the art of pressure control

The algorithm used as benchmark is based on physical considerations on steady state conditions in WDNs [12]. It aims to correct the local head loss coefficient ξ of the valve, which is an increasing function of α, as derived from the specific valve curve $\xi(\alpha)$ provided by the valve manufacturer. Then $\Delta\xi$, i.e. the variation of ξ applied by the regulator, is equal to:

$$\Delta\xi = K\frac{2gA^2}{Q^2}e \tag{8}$$

where A $[m^2]$ is the cross area of the pipe equipped with the valve. Q $[m^3/s]$ is the measured water flow in the same pipe. Finally, K is a constant that is tuned by trial and error. Once $\Delta\xi$ is computed, the $\alpha(\xi)$ curve can be used to define to new valve setting α. This controller is usually applied with control time steps of the order of magnitude of some minutes. The values of e and Q to be used for assessing $\Delta\xi$ are the average values measured during the previous control time step. For both case studies, the algorithm is applied with a time step of 180 s. In the following of the paper, this algorithm will be referred to as *P on ξ*.

Case study A

The results of simulations described in § 2 are reported in Table 1. The best value of the controller constant K is experimentally determined as $K = 0.862$. Figure 6 depicts the closed-loop simulation of a fire hydrant opening. Pressure is restored in about 600 s by *P on ξ* algorithm.

Demand Offset $[m^3/s]$	*Displacement Instants* $[\%]$	$\sum \lvert\Delta\alpha\rvert$ $[-]$	*Mean*$\lvert e(k)\rvert$ $[m]$
-0,03	0,68	3,17	2,31
-0,02	0,69	3,19	1,94
-0,01	0,70	3,24	1,68
0	0,71	3,33	1,50
0,01	0,73	3,69	1,25
0,03	0,78	3,98	1,16
0,04	0,81	4,36	1,08
0,05	0,88	4,89	1,01

Table 1: Performance of *P on ξ* algorithm for different demand offsets.

Demand Profile	*Displacement Instants* $[\%]$	$\sum \lvert\Delta\alpha\rvert$ $[-]$	*Mean*$\lvert e(k)\rvert$ $[m]$
A	2	3.37	1.06
B	2.75	5.55	0.98

Table 2: Case Study B: Performance of *PI on ξ* algorithm for different demand profiles.

Case study B

Table 2 shows the results of simulations, with the two different demand profiles introduced in § 2. The controller constant was set to $K = 0.4$ to obtain the best results for Case Study B.

6. Pressure control strategies based on dynamic models

In this section different control strategies synthesized on linear dynamic models of the plant are introduced. All the presented algorithms use an approximated linear model identified around a suitable working point of the system under control.

6.1. Working points

The first step of a model-based synthesis is the definition of a nominal working point, typically an equilibrium of the system. When a mathematical description of the process is available in state-space form, it is possible to find its equilibria by requiring the state derivatives to be zero, when inputs are set to a constant value (i.e. by requiring a steady state condition to be reached). The mathematical modelling of the WDN introduced in § 3 allows the detailed description and simulation of the dynamics of the system, but is too complex to be put in state-space form. However, the nominal working point can be found experimentally by means of simulations.
For this purpose, a Multi-Input Single-Output (MISO) system must be considered in both case studies. Input signals are:

- $\alpha(t)$, the valve closure ($[-]$).
- $H(t)$, the source pressure head ($[m]$).

- $D_i(t)$, the water demand ($[m^3/s]$) at node i.

The output is the pressure $h(t)$ (expressed in $[m]$) measured at the desired point of the WDN.
Note that $\alpha(t)$ is the only control variable, since we assume no possibility of controlling the source pressure $H(t)$. Consequently, $H(t)$ and $D_i(t)$ represent stochastic disturbances acting on the process. Typical profiles of $H(t)$ and $D(t)$ are depicted in Figure 2 for Case Study A, with $D(t)$ the demand of the single demanding node. Figure 4 shows the profiles for Case Study B, with $D(t)$ representing the overall demand of the WDN, i.e.:

$$D(t) = \sum_{i=1}^{N_{nodes}} D_i(t) \tag{9}$$

where N_{nodes} is the number of demanding nodes in the WDN. In the definition of the working point, the average values of typical $H(t)$ and $D_i(t)$ profiles are considered as input to the system.

Case study A

The control goal in Case Study A is to perform a pressure regulation at $h_{sp} = 29\ m$ at the controlled node, which is placed in the middle of the pipe. Simulations allow to define the value of α which results in the desired pressure, when the exogenous inputs acting on the system are the average value of the source pressure head $H(t)$ and the average value of the demand $D(t)$. The working point for Case Study A is then defined by the tuple $WP_A = (\overline{\alpha}, \overline{H}, \overline{D}, \overline{h})$:

$$WP_A = \begin{cases} \overline{\alpha} = 0.694 \\ \overline{H} = 50\ m \\ \overline{D} = 0.1\ m^3/s \\ \overline{h} = 29\ m \end{cases} \tag{10}$$

Case study B

The control goal in Case Study B is to perform the pressure regulation at $h_{sp} = 25\ m$ at the controlled node, which coincides with node 1. The average value of the source pressure head and demand must be used in the simulations. Note that, in the case of multiple demanding nodes, it is necessary to consider the average value of each demand profile $D_i(t)$. The tuple $WP_B = (\overline{\alpha}, \overline{H}, \overline{D}_1, ..., \overline{D}_{N_{nodes}}, \overline{h})$ is then the working point for Case Study B:

$$WP_B = \begin{cases} \overline{\alpha} = 0.619 \\ \overline{H} = 39.6\ m \\ \overline{D}_1 = 0.0014\ m^3/s \\ ... \\ \overline{D}_{N_{nodes}} = 0.0007\ m^3/s \\ \overline{h} = 25\ m \end{cases} \tag{11}$$

Remark: Demand profiles A and B share the same average values for each $D_i(t)$, therefore it is not necessary to define two different working points for Case Study B.

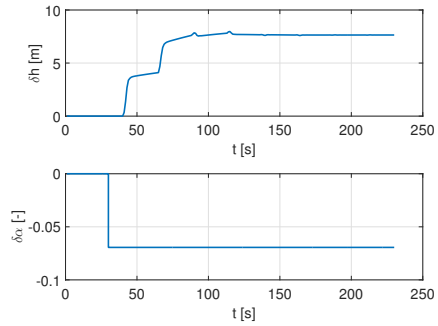

Figure 7: Case Study A: identification data. Top: pressure variation $\delta h(t)$. Bottom: valve variation $\delta\alpha(t)$.

6.2. Dynamic models

The synthesis of regulators requires a dynamic model relating the valve closure $\alpha(t)$ to the pressure $h(t)$. Since analytical linearization is too complex in view of the complexity of the nonlinear model, black-box identification, based on simulated data collected on the simulator, has been exploited for the definition of a local model describing the dynamics of the system around the equilibrium. The identification phase is set-up as follows:

- *Simulation of a step response of the WDN around the working point.* The system is first brought around the desired working point. Then, once a stedy state condition is reached, a 10% step variation of α is applied (the valve speed limit is disabled for this simulation). Let $\Delta\alpha_{step}$ be the amplitude of the step.

- *Buildup of input-output identification data.* A local model must be identified, therefore it is necessary to construct variation signals $\delta\alpha(t) = \alpha(t) - \overline{\alpha}$ and $\delta h(t) = h(t) - \overline{h}$ as input-output data. The former signal represents the input of the linearised system, the latter its output.

- *Definition of the structure of the model.* The structure of the local model must be chosen according to the behaviour of the step response $\delta\alpha(t)$.

- *Identification of the parameters of the model.* Matlab Identification Toolbox [30] allows to use input-output data to optimise the values of parameters, to provide the best fit between model prediction and identification data.

- *Validation.* The model prediction is compared against simulations of step responses of the WDN. Different step amplitudes are used to validate the model.

Case study A

A step response simulation around WP_A allows to obtain the input-output identification data shown in Figure 7. The step response does not show any overshoot, inverse response or oscillation. Still, a pure delay is present, and coincides with the time required by the pressure wave generated from the valve to reach the pressure sensor. The celerity of the wave is known, therefore the delay τ_a can be computed as:

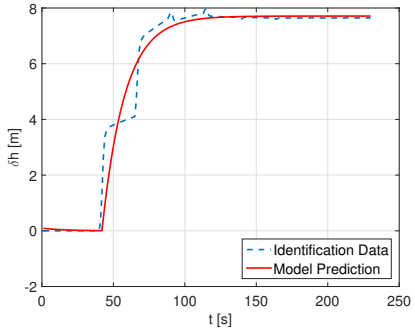

Figure 8: Case Study A: comparison of model and system output with identification data.

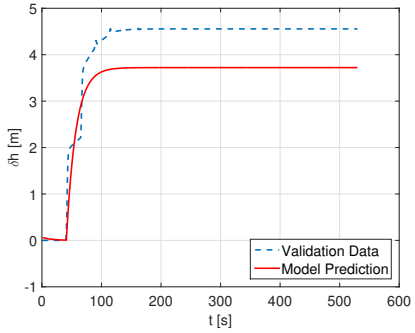

Figure 9: Case Study A: comparison of model and system output with validation data.

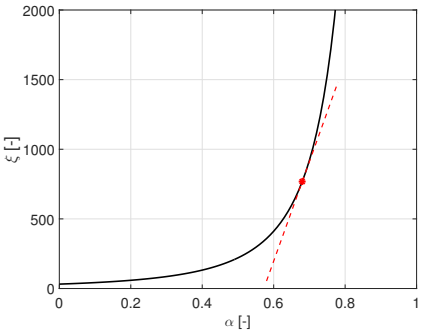

Figure 10: The local loss coefficient ξ as function of the valve closure α and the straight line tangent to the curve in the working point.

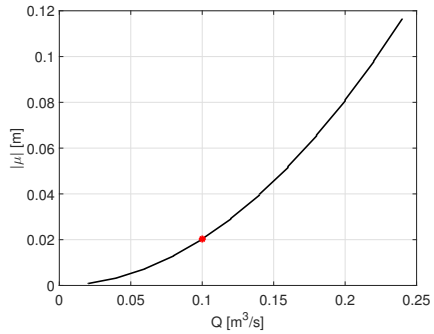

Figure 11: Absolute value of the gain of the linearised system μ_a as function of the flow Q.

$$\tau_a = \frac{L_{v-s}}{c} \tag{12}$$

where L_{v-s} is the distance between the valve and the sensor and c is the celerity of the wave.

The structure chosen for the model (a continuous time transfer function, with s the Laplace variable) and the values of its parameters are reported in (13). Figure 8 shows a comparison between the model output and the identification data.

$$G_a(s) = \frac{\mu_a e^{-s\tau_a}}{1+sT_a}$$

$$\begin{aligned} \mu_a &= -107.27\ m \\ T_a &= 16\ s \\ \tau_a &= 11\ s \end{aligned} \tag{13}$$

Validation is performed by simulating the step response with different step amplitudes and comparing the results to the response predicted by the model. In particular, Figure 9 shows the response to a 5% step in α. The model does not exactly predict the gain of the system, due to the presence of some nonlinearities.

Let us consider (6), where α does not directly affect the pressure loss, but appears through ξ. The relation between ξ and α, depicted in Figure 10, is strongly nonlinear. A formal linearisation procedure would approximate the relation with the slope of the tangent to the curve in correspondence of the working point ($\frac{d\xi}{d\alpha}|_{\alpha=\overline{\alpha}}$). The proposed procedure approximates it as $\frac{\Delta\xi}{\Delta\alpha_{step}}$, which depends on the amplitude of the step applied during the identification phase.

Equation (4) shows instead that the pressure variation generated by a step $\Delta\alpha_{step}$ also depends on the flow Q. In particular, the absolute value of the pressure variation increases with the square of the flow. Figure 11 depicts the relation between the absolute value of the gain of the linearised system ($|\mu_a|$) and the flow Q. The relation is obtained by repeating the identification procedure at different values of Q, with same values of $\overline{\alpha}$ and $\Delta\alpha_{step}$.

Nevertheless, the two nonlinearities do not cumulate, but are likely to cancel each other in closed-loop. In fact, whenever the flow Q increases, the pressure h would decrease. The valve closure α must then decrease to compensate for the pressure loss. An increase in Q then results in a decrease in α. When considering this effect in terms of gain of the linearised system, an increase in Q means an increase in the gain, but the resulting decrease in α means a decrease in the gain. On the other hand, if Q decreases, the pressure h increases and α must be increased, thus the two effects still compensate each other. Still, in case of $\alpha \approx 1$, the ξ nonlinearity is dominant and is not mitigated by the Q one. Note that this is not likely to happen in real situations: $\alpha \approx 1$ would be required when $D \approx 0$, but this never happens due to leakage. On the contrary, when $\alpha \approx 0$, the Q nonlinearity dominates. In view of these considerations, it is still important to synthesise regulators providing sufficient margin of robustnes, and setup simulations to test the robustness of the regulators.

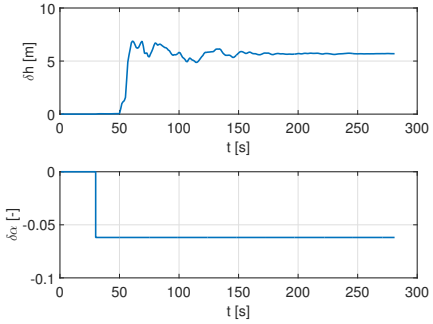

Figure 12: Identification data for Case Study B. Top: pressure variation $\delta h(t)$. Bottom: valve variation $\delta\alpha(t)$.

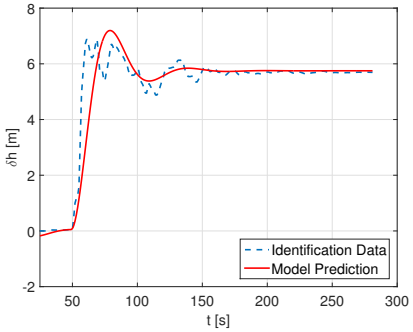

Figure 13: Case Study B: Comparison of model and system output with identification data.

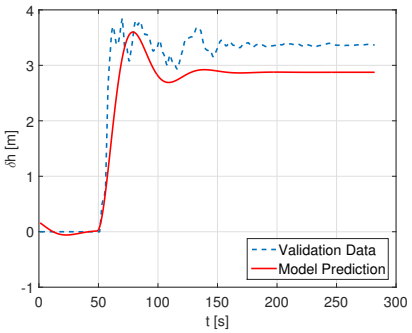

Figure 14: Case Study B: Comparison of model and system output with validation data.

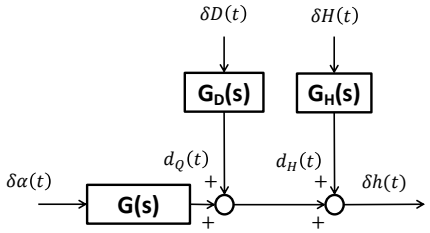

Figure 15: SISO system for control purposes.

Case study B

The previous procedure can be applied to Case Study B. Figure 12 shows the identification step response around WP_B. Some oscillations are present in the response, due to the effect of pressure waves coming from different paths of the WDN. This motivates the introduction of a second order transfer function model with complex conjugate poles. The pure delay is still present, but its computation can no longer be made by means of a structural analysis of the WDN, and must be treated as a parameter for the identification problem. The overall structure chosen for the model and the values of its parameters are reported in (14). Figure 13 shows a comparison between the model output and the identification data. Validation is depicted in Figure 14. The applied step is $\Delta\alpha_{step} = 5\%$ (a 10% step was used for identification). The considerations about gain nonlinearities which were introduced for Case Study A still hold for Case Study B.

$$G_b(s) = \frac{\mu_b e^{-s\tau_b}}{1+2\zeta_b s/\omega_b+s^2/\omega_b^2}$$

$$\begin{aligned} \mu_b &= -92.86\ m \\ \zeta_b &= 0.4 \\ \omega_b &= 0.1\ rad/s \\ \tau_b &= 19\ s \end{aligned} \tag{14}$$

6.3. Control

The main goal is regulation to the setpoint h_{sp} of the pressure $h(t)$, in presence of process disturbances generated by the effect of exogenous inputs $H(t)$ and $D_i(t)$. In this situation, it is possible to refer to a Single-Input Single-Output (SISO) system, whose behaviour around the working point can be described by the local, linear models derived in § 6.2. Regulators are then synthesised on the basis of $G_a(s)$ and $G_b(s)$, requiring the closed-loop bandwidth to be the largest possible, while providing robustness to gain and phase variations. The SISO system and the linear framework considered for the control design are depicted in Figure 15, where $\delta H(t)$ and $\delta D(t)$ are the source pressure and nodal demand variation signals from their working point values. Then $d_H(t)$ is the disturbance generated by $\delta H(t)$ through the dynamic relation $G_H(s)$, and $d_Q(t)$ the disturbance generated by $\delta D(t)$ through the dynamic relation $G_D(s)$. Note that the knowledge of $G_H(s)$ and $G_D(s)$ is not required by the control algorithms proposed in this work.

Note that, every time the value of D_i changes, a pressure wave is generated from the corresponding demanding node and propagates throughout the WDN. A reflected wave is generated as well when the primary one reaches the end of a pipe or the control valve. This effect is particularly important in Case Study A, since the wave propagates and gets reflected through a single pipe. The same holds every time the value of α changes, with the primary wave propagating from the valve towards the demanding node.

The same effect is present in the more complex WDN considered for case Study B. Still, due to the presence of many possible paths for the pressure waves, the power is distributed over a number of harmonics and is expected to have less impact

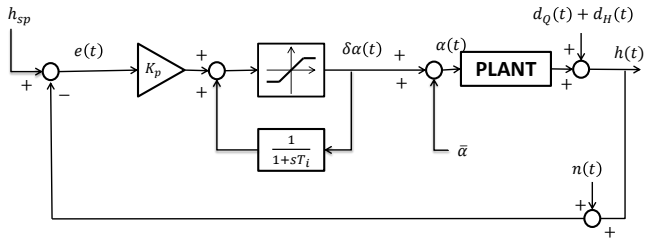

Figure 16: Antiwindup control scheme for *PI* regulators.

on closed-loop performance. Some realistic measurement noise $n(t)$ is present in Case Study B as well.

All regulators are implemented in a discrete-time way, by exploiting the full capability of the measurement system in terms of sampling time, which results in $T_s = 1\ s$. Discretisation of regulators is performed with *Tustin* method to guarantee that the stability is preserved (all asymptotically stable/stable continuous time poles are respectively mapped into asymptotically stable/stable discrete time poles). The design and test of the different control schemes based on the dynamic model derived in § 6.2 are presented in the following subsections.

6.4. PI regulators

A Proportional-Integral (PI) control action $u(t)$ can be expressed as follows [31]:

$$u(t) = K_p e(t) + K_i \int e(t)dt \tag{15}$$

where $e(t)$ is the error signal. Moving to the *Laplace* domain, one has:

$$U(s) = K_p E(s) + \frac{K_i}{s} E(s) \tag{16}$$

with s the Laplace variable, $F(s)$ the Laplace transform of a generic time domain signal $f(t)$. The transfer function of the regulator can be written as follows:

$$R(s) = \frac{U(s)}{E(s)} = K_p + \frac{K_i}{s} = \frac{K_p s + K_i}{s} = K_i \frac{1 + s\frac{K_p}{K_i}}{s} \tag{17}$$

By defining $T_i = \frac{K_p}{K_i}$ and $\mu_r = K_i$, one has:

$$R(s) = \mu_r \frac{1 + sT_i}{s} \tag{18}$$

By properly shaping the loop transfer function $L(s) = G(s)R(s)$, it is possible to cope with the different control requirements. Note that, when no derivative action is present, an integrator in $L(s)$ ensures perfect tracking of step reference signals and complete rejection of step process disturbances. Still, the presence of a saturation of the control action (recall $\alpha \in [0; 1]$) calls for an antiwindup implementation of the PI regulator, to avoid undershoots/overshoots which may completely empty the WDN. The overall control scheme is depicted in Figure 16. Note that the model of the saturation affects $\delta\alpha$. It must be therefore implemented as $\delta\alpha \in [1 - \overline{\alpha}; -\overline{\alpha}]$. Stability of the resulting closed-loop systems can be assessed by means of the *Bode Criterion*, which is reported in Theorem 1 [31].

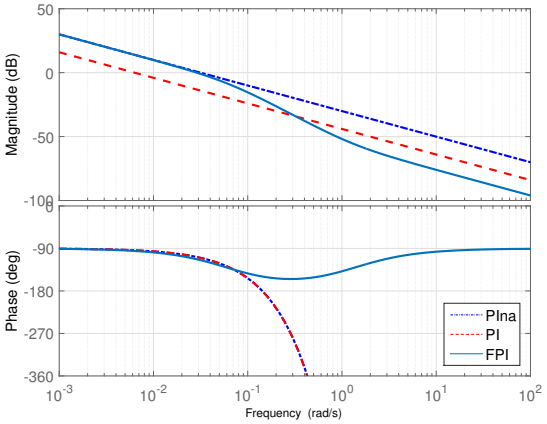

Figure 17: Case Study A: design of loop functions for PI_{na}, *PI* and *FPI* regulators.

Demand Offset $[m^3/s]$	*Displacement Instants* [%]	$\sum\|\Delta\alpha\|$ [−]	*Mean*$\|e(k)\|$ $[m]$
-0,03	100	223,21	2,29
-0,02	100	169,05	1,73
-0,01	100	93,63	1,03
0	100	38,33	0,51
0,01	100	35,02	0,49
0,02	100	33,49	0,48
0,03	100	32,48	0,48
0,04	100	31,78	0,49
0,05	100	31,3	0,5

Table 3: Case Study A: performance of PI_{na} algorithm for different demand offsets.

Theorem 1. *Let $L(s)$ have poles with non-positive real part only, and let the Bode diagram of $|L(j\omega)|$ cross the 0 dB axis only once. Then, by defining as μ_L the gain of $L(s)$ and as ϕ_m the phase margin, the negative feedback system is asymptotically stable iif $\mu_L > 0$ and $\phi_m > 0$.*

Case study A

Let the model of the system be described by (13). It is then possible to set:

$$T_i = T_a \quad \mu_r = \frac{\omega_c}{\mu_a} \tag{19}$$

where ω_c is the desired closed-loop bandwidth expressed in rad/s.
The resulting loop transfer function $L(s)$ is reported in (20):

$$L(s) = \frac{\omega_c}{s} e^{-s\tau} \tag{20}$$

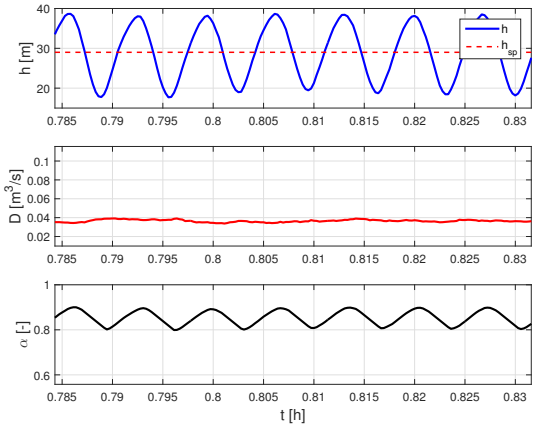

Figure 18: Case Study A: closed-loop simulation with PI_{na} and demand offset $-0.03\ m^3/s$. Top: pressure $h(t)$ and pressure setpoint h_{sp}. Middle: demand $D(t)$. Bottom: valve closure $\alpha(t)$.

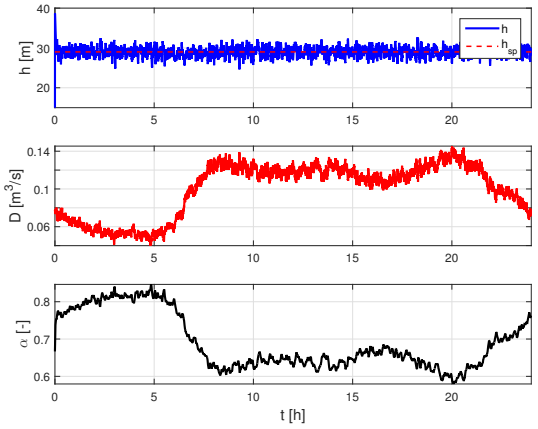

Figure 19: Case Study A: closed-loop simulation with PI algorithm. Top: pressure $h(t)$ and pressure setpoint h_{sp}. Middle: demand $D(t)$. Bottom: valve closure $\alpha(t)$.

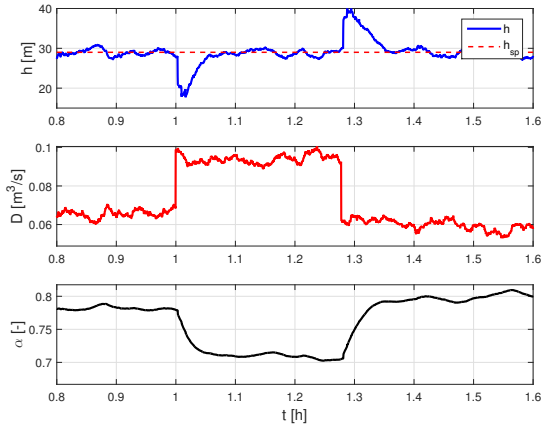

Figure 20: Case Study A: closed-loop simulation with PI algorithm and opening of a fire hydrant. Top: pressure $h(t)$ and pressure setpoint h_{sp}. Middle: demand $D(t)$. Bottom: valve closure $\alpha(t)$.

Demand Offset $[m^3/s]$	*Displacement Instants* $[\%]$	$\sum\lvert\Delta\alpha\rvert$ $[-]$	*Mean*$\lvert e(k)\rvert$ $[m]$
-0,03	100	8,57	1,12
-0,02	100	7,96	1,02
-0,01	100	7,55	0,94
0	100	7,24	0,89
0,01	100	7,01	0,85
0,02	100	6,83	0,82
0,03	100	6,7	0,8
0,04	100	6,62	0,78
0,05	100	6,56	0,78

Table 4: Case Study A: performance of PI algorithm for different demand offsets.

The only free design parameter is ω_c, which must be chosen according to the design specifications.

A first PI is tuned by requiring $\omega_c = 0.0314\ rad/s$. In the following, this algorithm will be referred to as PI_{na}. The resulting loop function $L(s)$ is depicted in Figure 17. The associated phase margin, including the effect of the pure delay, results $\phi_m = 70°$, ensuring robust stability of the closed-loop and very little oscillations in the closed-loop step response. Phase margin reduction due to discretisation is negligible.

Table 3 shows the results of closed-loop simulations with PI_{na}. Note that, for negative demand offset values, the cost of regulation grows very high and the regulation error gets worse. This is due to the presence of a pressure wave with frequency

$$f_w = \frac{1}{25} = 0.04\ Hz \tag{21}$$

propagating through the pipe. The effect is shown in Figure 18, with reference to a simulation with demand offset of $-0.03\ m^3/s$. Recall that a pressure wave is generated every time the valve setting α changes. Such wave propagates through the pipe and gets reflected once it reaches the demanding node, hitting the pressure sensor again while moving back towards the valve. When the controller tries to compensate for the pressure variation, a new wave is generated and reflected. In addition, with very low values of the demand $D(t)$, the regulator sets values of α which get close to 1. According to the effect of gain nonlinearities described in § 6.3, the ξ nonlinearity dominates and the gain of the process increases. This in turn means that the closed-loop bandwidth is enlarged and that the regulator tries to compensate the effect of the pressure wave propagating through the pipe, instead of filtering it. By doing so, other waves at the same frequency are generated. Other works instead suggest that the observed oscillations are the result of the phase margin reduction which occours due to the enlarged closed-loop bandwidth [8],[24],[25].

A retuning of the regulator is therefore necessary. A possibility is to reduce the closed-loop bandwidth. A second attempt is then made with $\omega_c = 0.0063\ rad/s$. The new phase margin is $\phi_m = 86°$ (phase margin reduction due to discretisation is negligible). The new PI will be referred to simply as PI. Results are reported in Table 4. Figure 19 shows the main signals of

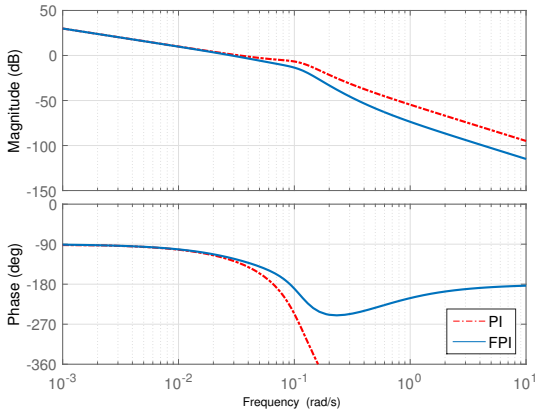

Figure 21: Case Study B: design of loop functions for *PI* and *FPI* regulators.

Demand Profile	*Displacement Instants* [%]	$\sum \lvert\Delta\alpha\rvert$ [−]	*Mean*$\lvert e(k)\rvert$ [*m*]
A	100	33.5	0.7
B	98	22.9	0.55

Table 5: Case Study B: Performance of *PI* algorithm for different demand profiles.

the control-loop for a whole day simulation with the nominal demand profile. Figure 20 shows the response of the system in presence of an additional step disturbance $D_s(t) = 0.03\ m^3/s$. This simulation mimics real situations, such as a sudden break of a pipe or the opening of a fire hydrant. The control system manages to bring the pressure back to the setpoint without any oscillation in about 300 s.

Case study B

For Case Study B, the local model of the system is reported in (14). A possible tuning is:

$$T_i = \frac{1}{2\omega_b} \quad \mu_r = \frac{\omega_c}{\mu_b} \tag{22}$$

with

$$\omega_c < \omega_b$$

.

The best results are obtained with $\omega_c = 0.0314\ rad/s$. Phase margin results $\phi_m = 48°$: the closed loop system is asymptotically stable but some damped oscillations may be present in the closed-loop step response. The Bode diagram of the loop function $L(s)$ is depicted in Figure 21 (phase margin reduction associated to the discretisation can be neglected). The proposed tuning tries to find a balance between phase margin and distance of $|L(j\omega)_{dB}|$ from the 0 dB axis right after ω_c. The phase margin must be sufficient to avoid wide oscillations in the closed-loop response and provide robustness to model uncertainty. The resonance peaks in $|L(j\omega)|_{dB}$ must not be too close to the 0 dB axis to provide robustness against the gain variations. Due to the resonance peak, an increase in the gain would in fact move ω_c at very high frequencies, and this may compromise the stability of the closed-loop system. The results of the simulations with the two demand profiles are presented in Table 5 and depicted in Figures 22 and 23.

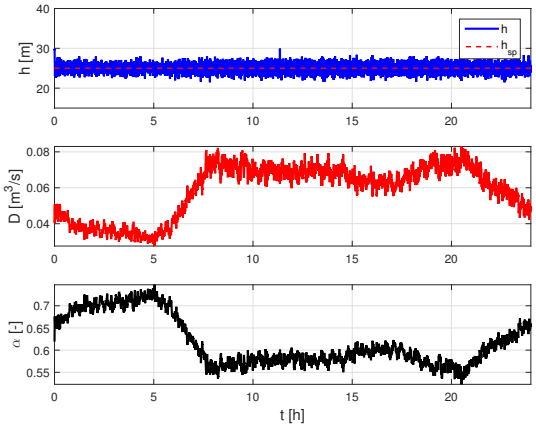

Figure 22: Case Study B: closed-loop simulation with *PI* algorithm and demand profile A. Top: pressure $h(t)$ and pressure setpoint h_{sp}. Middle: demand $D(t)$. Bottom: valve closure $\alpha(t)$.

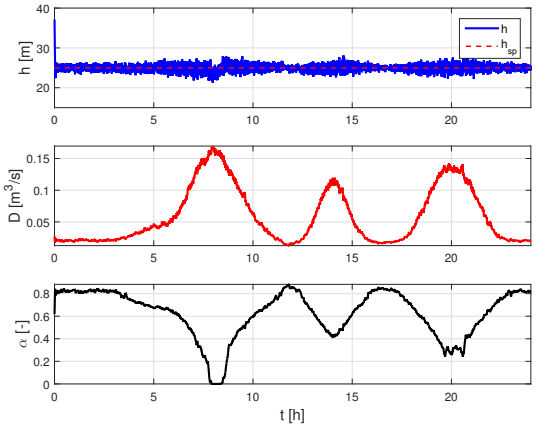

Figure 23: Case Study B: closed-loop simulation with *PI* algorithm and demand profile B. Top: pressure $h(t)$ and pressure setpoint h_{sp}. Middle: demand $D(t)$. Bottom: valve closure $\alpha(t)$.

6.5. *Filtered PI regulators and Smith predictor*

According to the previous considerations, it may be possible to improve the *PI* performance by introducing a low pass filter to enhance rejection of noise at frequency f_w. The overall regulator $R(s)$ can then be considered as the cascade of a *PI* controller, as described in § 6.4, and the filter given by the transfer function $R_f(s)$, reported in (23).

$$R_f(s) = \frac{(1 + sT_d)}{(1 + sT_f)} \tag{23}$$

When the filtering pole is placed just outside of the closed-loop bandwidth, the phase margin of the system can be reduced significantly. The zero of $R_f(s)$ can be used to reduce the phase margin loss. In the following of the paper, this algorithm will be referred to as *FPI* (Filtered PI). Since the system under control is characterised by the presence of a pure delay, it is also

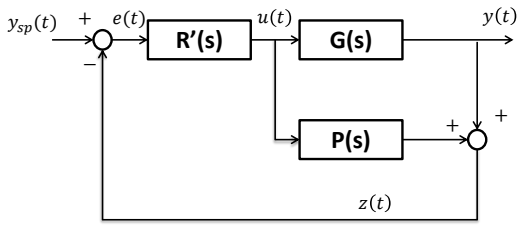

Figure 24: Control scheme with Smith Predictor.

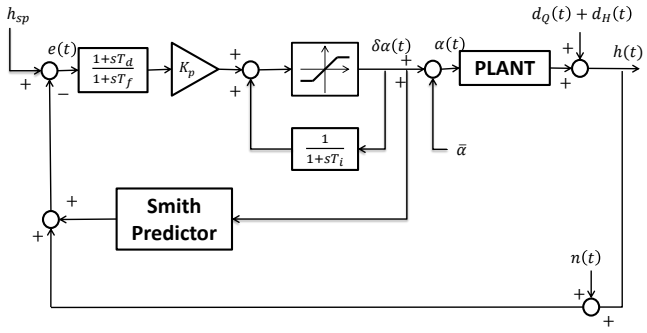

Figure 25: Antiwindup control scheme for FPI regulators with Smith Predictor.

possible to compensate for its effect on the phase margin by introducing a Smith Predictor (SP), which is now presented.

Consider an asymptotically stable SISO system with transfer function

$$G(s) = G'(s)e^{-s\tau} \tag{24}$$

where $G'(s)$ is a rational transfer function. Then, with reference to the control scheme in Figure 24, it is possible to neglect the presence of the pure delay $e^{-s\tau}$ in the design of the regulator $R'(s)$ when

$$P(s) = (1 - e^{-s\tau})G'(s) \tag{25}$$

The effect of the scheme is to obtain a feedback with a *prediction* $z(t) = y(t + \tau)$ of the controlled variable $y(t)$.

The overall control scheme for the FPI algorithm with antiwindup implementation and Smith Predictor is depicted in Figure 25.

Case study A

In Case Study A it is possible to compute the frequency f_w of the pressure wave as described in (21). The PI_{na} algorithm presented in § 6.4 can be extended to provide more rejection of noise at frequency f_w. The best design of the filter $R_f(s)$ is obtained by setting:

$$T_d = \frac{1}{5}\frac{1}{2\pi f_w} \quad T_f = 20T_d \tag{26}$$

which provides $30dB$ of rejection of the pressure wave. The bode diagram of the overall loop function $L(s)$ is reported in Figure 17. The closed-loop bandwidth is approximately $\omega_c = 0.0314\ rad/s$. Thanks to the Smith Predictor, the phase

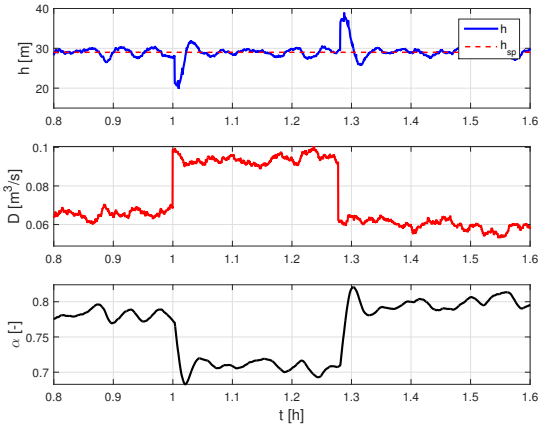

Figure 26: Case Study A: closed-loop simulation with FPI algorithm and opening of a fire hydrant. Top: pressure $h(t)$ and pressure setpoint h_{sp}. Middle: demand $D(t)$. Bottom: valve closure $\alpha(t)$.

Demand Profile $[m^3/s]$	*Displacement Instants* $[\%]$	$\sum\|\Delta\alpha\|$ $[-]$	*Mean*$\|e(k)\|$ $[m]$
-0,03	100	15	0,74
-0,02	100	14,1	0,69
-0,01	100	13,46	0,66
0	100	12,98	0,64
0,01	100	12,62	0,62
0,02	100	12,34	0,6
0,03	100	12,18	0,56
0,04	100	12,11	0,59
0,05	100	12,11	0,59

Table 6: Case Study A: performance of FPI algorithm for different demand offsets.

margin results $\phi_m = 67°$ (by neglecting the effect of discretisation), ensuring robust stability of the closed-loop and very little oscillations in the closed-loop step response. Note that, in contrast with the closed-loop bandwidth reduction introduced for the PI algorithm, the proposed filter design limits the closed-loop bandwidth in case of increase in the process gain, while keeping the nominal closed-loop bandwidth almost unchanged. Result of whole day simulations are reported in Table 6. Simulation of fire hydrant opening is instead shown in Figure 26. Regulation to h_{sp} is faster than the PI case but shows a little overshoot/undershoot. In the following, this algorithm will be simply referred to as FPI.

Case study B

The WDN considered in Case Study B shows a complex topology with many possible paths connecting the control valve to the controlled node. Cycles are also present. Many pressure waves are therefore generated when a variation of the status of the valve occurs. In addition, each demanding node generates waves which propagate through the network. It is then very difficult to identify the frequencies of such waves. Still, a possi-

Demand Profile	*Displacement Instants* [%]	$\sum \lvert\Delta\alpha\rvert$ [−]	*Mean*$\lvert e(k)\rvert$ [m]
A	100	11.4	0.74
B	98	9.6	0.62

Table 7: Case Study B: Performance of FPI algorithm for different demand profiles.

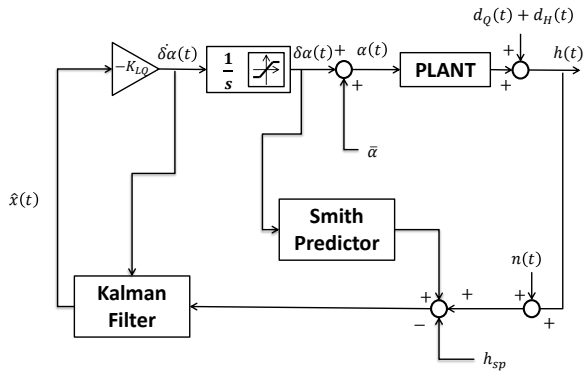

Figure 27: Control scheme for the LQG regulator, featuring integral action and Smith Predictor

ble design for the $R_f(s)$ placing the filtering pole right after the closed-loop bandwidth and then placing the zero in an arbitrary position to improve the phase margin. The Smith Predictor described in the previous section is still included in the design. Let therefore:

$$T_f = \frac{0.6}{\omega_c} \quad T_d = 0.1T_f \tag{27}$$

With the PI tuned as in § 6.4, with $\omega_c = 0.0314\ rad/s$, the overall regulator provides a phase margin $\phi_m = 59°$. The effect of discretisation on the phase margin is negligible. The corresponding loop function is reported in Figure 21. A comparison of the loop functions obtained with the PI and the FPI algorithms highlights that the FPI results in a reduced magnitude in correspondence of the resonance peak, which is outside of the closed-loop bandwidth and in turn present in the control sensitivity function as well. The overall effect is a reduction of the associated actuator oscillations. Table 7 reports the results of simulations of the WDN in closed loop with the FPI algorithm.

6.6. Linear Quadratic Gaussian control

Linear Quadratic Gaussian (LQG) control is one of the most common optimal control techniques. Optimal control allows to formulate control problems as optimisation ones, explicitly taking into account cost/benefit trade-offs in the synthesis of the controller. In particular, LQG control is the combination of a Linear Quadratic (LQ) state-feedback controller and a Kalman Filter (KF) for estimation of nonmeasurable states. In particular, the LQG schemes developed in this work features a discrete time, infinite horizon LQ regulator and a steady-state KF. The main results of infinite horizon LQ control are summarised in Theorem 2, while Theorem 3 discusses the steady-state KF [32].

Theorem 2. Consider a linear, discrete time system described by:

$$\mathbf{x}(k+1) = \mathbf{A}\mathbf{x}(k) + \mathbf{B}\mathbf{u}(k) \tag{28}$$

and the infinite horizon quadratic cost function:

$$\begin{aligned} &J = \textstyle\sum_{k=0}^{\infty}(\mathbf{x}^\top(k)\mathbf{Q}\mathbf{x}(k) + \mathbf{u}^\top(k)\mathbf{R}\mathbf{u}(k)) \\ &\text{with} \\ &\mathbf{Q} \geq 0 \quad \mathbf{R} > 0 \end{aligned} \tag{29}$$

If the pair $(\mathbf{A}, \mathbf{B})$ is reachable, and the pair $(\mathbf{A}, \mathbf{Cq})$ is observable, with $\mathbf{Q} = \mathbf{Cq}^\top\mathbf{Cq}$,
then, the optimal control law is given by

$$\mathbf{u}(k) = -\mathbf{K}_{LQ}\mathbf{x}(k) \tag{30}$$

with

$$\mathbf{K} = (\mathbf{R} + \mathbf{B}^\top\overline{\mathbf{P}}\mathbf{B})^{-1}\mathbf{B}^\top\overline{\mathbf{P}}\mathbf{A} \tag{31}$$

where $\overline{\mathbf{P}}$ is the unique positive definite solution of the stationary Riccati Equation

$$\mathbf{P}{=}\mathbf{A}^\top\mathbf{P}\mathbf{A} + \mathbf{Q} - \mathbf{A}^\top\mathbf{P}\mathbf{B}(\mathbf{R} + \mathbf{B}^\top\mathbf{P}\mathbf{B})^{-1}\mathbf{B}^\top\mathbf{P}\mathbf{A} \tag{32}$$

The closed-loop system

$$\mathbf{x}(k+1) = (\mathbf{A} - \mathbf{B}\mathbf{K}_{LQ})\mathbf{x}(k) \tag{33}$$

is asymptotically stable.

Theorem 3. Assume that the considered system is described by:

$$\begin{cases} \mathbf{x}(k+1) = \mathbf{A}\mathbf{x}(k) + \mathbf{B}\mathbf{u}(k) + \mathbf{w}(k) \quad \mathbf{x}(0) = \mathbf{x}_0 \\ y(k) = \mathbf{C}\mathbf{x}(k) + n(k) \end{cases} \tag{34}$$

with $\mathbf{w}(k)$ and $n(k)$ respectively process and measurement noise. Let $\mathbf{w}(k)$ be white, Gaussian with zero mean and covariance $\mathbf{Q}_k$. Analogously, let $n(k)$ be white, Gaussian with zero mean and covariance R_k. Let also assume that the two noises are not correlated.
If the pair $(\mathbf{A}, \mathbf{Bq})$, with $\mathbf{Bq}$ such that $\mathbf{Q}_k = \mathbf{Bq}^\top\mathbf{Bq}$, is reachable and that the pair $(\mathbf{A}, \mathbf{C})$ is observable, the optimal state estimator is then given by:

$$\begin{aligned} \hat{\mathbf{x}}(k+1|k+1) = \mathbf{A}\hat{\mathbf{x}}(k|k) + \mathbf{B}\mathbf{u}(k) + \\ +\mathbf{L}[y(k+1) - \mathbf{C}(\mathbf{A}\hat{\mathbf{x}}(k|k) + \mathbf{B}\mathbf{u}(k))] \end{aligned} \tag{35}$$

with

$$\mathbf{L} = \overline{\mathbf{P}}\mathbf{C}^\top[\mathbf{C}\overline{\mathbf{P}}\mathbf{C}^\top + R_k]^{-1} \tag{36}$$

where $\overline{\mathbf{P}}$ is the unique positive definite solution of the stationary Riccati Equation

$$\mathbf{P} = \mathbf{A}\mathbf{P}\mathbf{A}^\top + \mathbf{Q}_k - \mathbf{A}\mathbf{P}\mathbf{C}^\top[\mathbf{C}\mathbf{P}\mathbf{C}^\top + R_k]^{-1}\mathbf{C}\mathbf{P}\mathbf{A} \tag{37}$$

The estimator is asymptotically stable, i.e. the eigenvalues of $(\mathbf{A} - \mathbf{LC})$ have modulus less than 1. Note that the eigenvalues

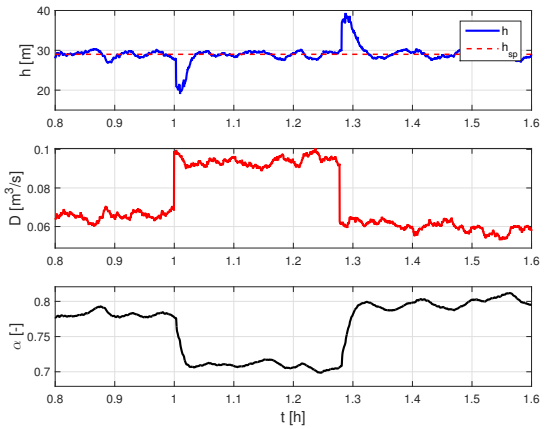

Figure 28: Case Study A: closed-loop simulation with *ILQG* algorithm and opening of a fire hydrant. Top: pressure $h(t)$ and pressure setpoint h_{sp}. Middle: demand $D(t)$. Bottom: valve closure $\alpha(t)$.

of the overall closed-loop system are those of $(\mathbf{A} - \mathbf{B}\mathbf{K}_{LQ})$ and of $(\mathbf{A} - \mathbf{L}\mathbf{C})$, so that the closed-loop stability is guaranteed.

Figure 27 shows the overall closed-loop setup for the implementation of the *LQG* control used in this paper. As for *PI* and *FPI* algorithms, the regulator is tuned according to linear models derived in § 6.2. Note that an integrator is introduced in the loop, providing a twofold contribution. On one hand, it allows to synthesise the LQ regulator with control action u coinciding with the derivative of the valve closure variation $\delta\alpha$. This in turn means that the derivative appears (in its discrete-time version) in the cost function, providing a more direct way to weight the performance metric $\sum|\Delta\alpha|$. On the other hand, with a SISO system without any derivative action, the presence of the integrator in the control loop ensures complete rejection of step process disturbances and perfect tracking of step references. Accumulation in the integrator is limited to the interval $[1-\overline{\alpha}; -\overline{\alpha}]$, to account for saturation of the control action and avoid integral windup.
Let $\mathbf{A}$, $\mathbf{B}$, and $\mathbf{C}$ be a realisation of (13) or (14). To introduce the integral action as described in Figure 27, the system is extended as:

$$\mathcal{A} = \begin{bmatrix} 0 & 0 \\ \mathbf{B} & \mathbf{A} \end{bmatrix} \quad \mathcal{B} = \begin{bmatrix} 1 \\ 0 \end{bmatrix} \quad C = \begin{bmatrix} 0 & \mathbf{C} \end{bmatrix} \tag{38}$$

The LQ and KF are then synthesised over the extended system $(\mathcal{A}, \mathcal{B}, C)$, discretised with step of 1 s and a Zero-Order Hold algorithm. The control scheme also features the Smith Predictor developed in § 6.5 for pure delay compensation. In the following of this work, this algorithm will be denoted as *ILQG*.

Case study A

Simulations with the water distribution system of Case Study A and *ILQG* algorithm provided the results shown in Table 8. Simulation of hydrant opening is depicted in Figure 28. Regulation to the setpoint is performed in about 250 s, with no oscillations in the response. The values of tuning parameters are:

Demand Profile $[m^3/s]$	*Displacement Instants* [%]	$\sum\|\Delta\alpha\|$ [−]	*Mean*$\|e(k)\|$ [*m*]
-0,03	100	13,4	0,84
-0,02	100	12,42	0,77
-0,01	100	11,77	0,73
0	100	11,32	0,7
0,01	100	11	0,68
0,02	100	10,75	0,66
0,03	100	10,6	0,65
0,04	100	10,5	0,65
0,05	100	10,5	0,65

Table 8: Case Study A: performance of *ILQG* algorithm for different demand offsets.

Demand Profile	*Displacement Instants* [%]	$\sum\|\Delta\alpha\|$ [−]	*Mean*$\|e(k)\|$ [*m*]
A	100	20	0.7
B	98	15	0.6

Table 9: Case Study B: Performance of *ILQG* algorithm for different demand profiles.

$$\mathbf{Q} = \begin{bmatrix} 10^{-4} & 0 \\ 0 & 10^{-8} \end{bmatrix} \quad \mathbf{R} = 1 \quad \mathbf{Q}_k = 0.005\mathbf{I}_{2\times 2} \quad R_k = 1$$

where the non-zero elements in $\mathbf{Q}$ weight respectively the state of the integrator and the state of the linearised system.

Case study B

For the WDN considered in case Study B, the best results are obtained with

$$\mathbf{Q} = \begin{bmatrix} 10^{-3} & 0 & 0 \\ 0 & 10^{-8} & 0 \\ 0 & 0 & 10^{-8} \end{bmatrix} \quad \mathbf{R} = 1 \quad \mathbf{Q}_k = 0.00005\mathbf{I}_{3\times 3} \quad R_k = 1$$

Performance metrics are reported in Table 9.

6.7. Linear Quadratic Gaussian control with shaping functions

Note that, for Case Study A, it is particularly interesting to bring in the *LQG* algorithm the same concepts introduced with the *FPI* one: an enhanced filtering at frequency f_w, and a limitation on the increase in the closed-loop bandwidth in case of increased gain of the process (see § 6.5). This result can be achieved by means of a control scheme with disturbances pre-filtering, as in Figure 29.
Let v_d, v_{n1}, v_{n2} be uncorrelated white noises, and let S_d and S_n be asymptotically stable systems producing the stationary

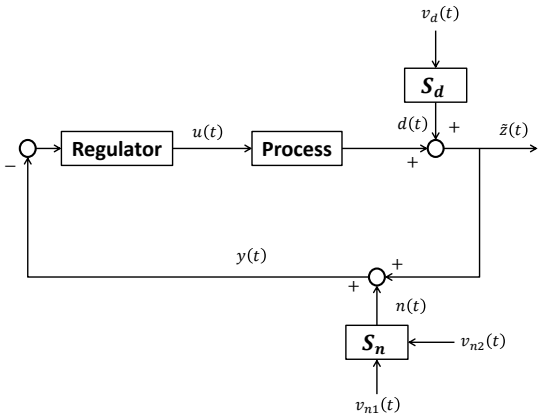

Figure 29: Control scheme for LQG control with disturbances prefiltering.

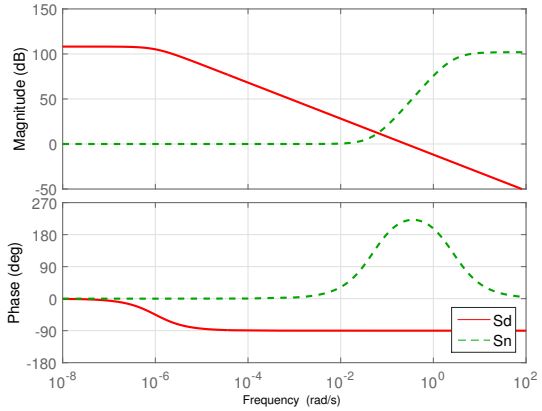

Figure 30: Shaping functions used for disturbances prefiltering.

noises $d(t)$ and $n(t)$. The process is described by:

$$\begin{cases} \dot{\mathbf{x}}(t) = \mathcal{A}\mathbf{x}(t) + \mathcal{B}u(t) \\ \tilde{z}(t) = C\mathbf{x}(t) + d(t) \\ y(t) = \tilde{z}(t) + n(t) \end{cases} \tag{39}$$

while S_d and S_n are described by:

$$\begin{cases} \dot{\mathbf{x}}_d(t) = \mathbf{A}_d\mathbf{x}_d(t) + \mathbf{B}_d v_d(t) \\ d(t) = \mathbf{C}_d\mathbf{x}_d(t) \end{cases} \tag{40}$$

and

$$\begin{cases} \dot{\mathbf{x}}_n(t) = \mathbf{A}_n\mathbf{x}_n(t) + \mathbf{B}_n v_{n1}(t) \\ n(t) = \mathbf{C}_n\mathbf{x}_n(t) + v_{n2}(t) \end{cases} \tag{41}$$

Now define:

$$\overline{\mathbf{x}}(t) = \begin{bmatrix} \mathbf{x}(t) \\ \mathbf{x}_d(t) \\ \mathbf{x}_n(t) \end{bmatrix} \quad \overline{\mathcal{A}} = \begin{bmatrix} \mathcal{A} & 0 & 0 \\ 0 & A_d & 0 \\ 0 & 0 & A_n \end{bmatrix} \quad \overline{\mathcal{B}} = \begin{bmatrix} \mathcal{B} \\ 0 \\ 0 \end{bmatrix} \tag{42}$$

$$\overline{\mathbf{v}}(t) = \begin{bmatrix} 0 & 0 \\ B_d & 0 \\ 0 & B_n \end{bmatrix} \begin{bmatrix} v_d(t) \\ v_{n1}(t) \end{bmatrix} \quad \overline{C} = \begin{bmatrix} C & C_d & C_n \end{bmatrix}$$

and the enlarged system:

$$\begin{cases} \dot{\overline{\mathbf{x}}}(t) = \overline{\mathcal{A}}\overline{\mathbf{x}}(t) + \overline{\mathcal{B}}u(t) + \overline{\mathbf{v}}(t) \\ y(t) = \overline{C}\overline{\mathbf{x}}(t) + v_{n2}(t) \end{cases} \tag{43}$$

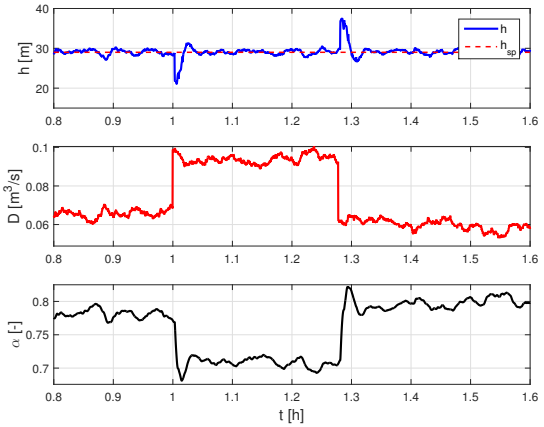

Figure 31: Case Study A: closed-loop simulation with $ILQG - SF$ algorithm and opening of a fire hydrant. Top: pressure $h(t)$ and pressure setpoint h_{sp}. Middle: demand $D(t)$. Bottom: valve closure $\alpha(t)$.

Demand Profile $[m^3/s]$	*Displacement Instants* [%]	$\sum\lvert\Delta\alpha\rvert$ [−]	*Mean*$\lvert e(k)\rvert$ [*m*]
-0,03	100	23	0,56
-0,02	100	22,1	0,53
-0,01	100	21,47	0,52
0	100	21	0,51
0,01	100	20,73	0,51
0,02	100	20,5	0,51
0,03	100	20,37	0,51
0,04	100	20,36	0,51
0,05	100	20	0,52

Table 10: Case Study A: performance of $ILQG - SF$ algorithm for different demand offsets.

Assuming that the covariance $Q_{k_{n2}}$ of v_{n2} is positive definite, then (43) fulfils the conditions required for the design of a stabilizing *LQG* regulator.
This algorithm is implemented on a discretised version of (43) and will be referred to as $ILQG - SF$. Shaping functions S_d and S_n can be chosen to place the power of measurement noise $n(t)$ from f_w towards higher frequencies and process noise $d(t)$ towards lower frequencies. Figure 30 depicts the chosen shapes and (44) reports the mathematical expressions.

$$\begin{aligned} \omega_w &= 2\pi f_w \\ S_d(s) &= \frac{\omega_w\, 10^6}{(1+s10^6)} \\ S_n(s) &= \frac{(1+s/(5\omega_w))^3}{(1+s/(0.1\omega_w))^3} \end{aligned} \tag{44}$$

With weights reported in (45), the regulation error improves significantly.

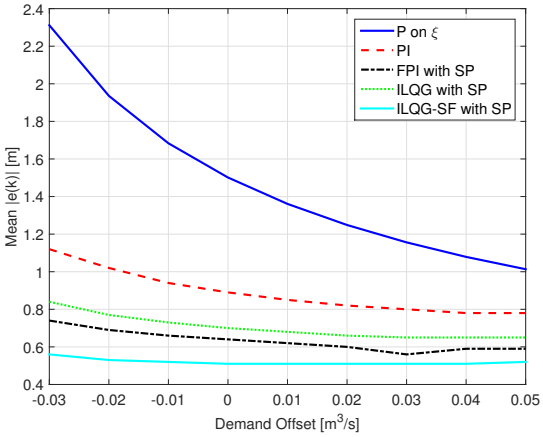

Figure 32: Case Study A: regulation error as function of the demand offset.

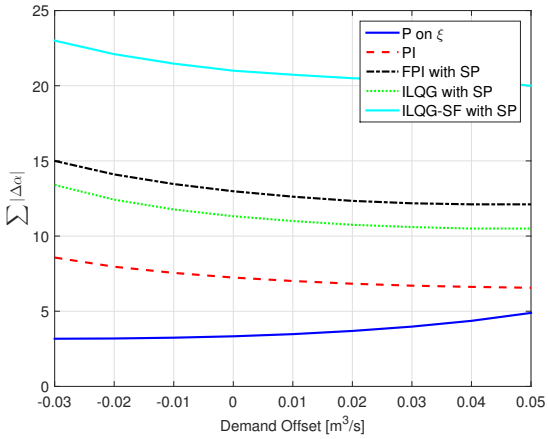

Figure 33: Case Study A: cost of control as function of the demand offset.

$$\mathbf{Q} = \begin{bmatrix} 1 & 0 & 0 & 0 & 0 & 0 \\ 0 & 10^{-12} & 0 & 0 & 0 & 0 \\ 0 & 0 & 0.26 & 0 & 0 & 0 \\ 0 & 0 & 0 & 0 & 0 & 0 \\ 0 & 0 & 0 & 0 & 0 & 0 \\ 0 & 0 & 0 & 0 & 0 & 0 \end{bmatrix} \quad R = 1 \qquad (45)$$

$$\mathbf{Q}_k = 0.05\mathbf{I}_{6\times 6} \quad R_k = 1$$

Performance metrics are reported in Table 10. Figure 31 shows the fire hydrant opening simulation. Regulation is slightly faster than the standard *ILQG* case, but shows some minor overshoot.

7. Analysis of results

The results of simulations introduced in § 5 and § 6 are now discussed and compared. To make comparison easier, results of Case Study A are reported in Figure 32 and Figure 33, where respectively the regulation error ($Mean|e(k)|$) and the cost of control ($\sum|\Delta\alpha|$) are plot as function of the demand offset. Note that regulators were tuned to obtain the best regulation error first. Then, if possible, tuning was changed to improve the control cost without degrading the regulation error. All the algorithms accounting for the dynamics of the system work with a control sampling time of 1 s, trying to compensate for the instantaneous variations of the pressure generated by demand and source pressure variations. The percentage of displacement instants is therefore always 100%. All these algorithms outperform the *PI on ξ* algorithm in term of regulation error. Note that *PI on ξ* regulation performance suffers more from demand offset variations, while the other algorithms provide more constant results. The $ILQG-SF$ stands out, providing the best regulation error, with very little variations due to the demand offset. FPI and $ILQG$ follow with similar performance. The *PI* algorithm could not properly rejects pressure wave noise and could only be applied with a reduced closed-loop bandwidth, thus is the less performing algorithm of the family. As expected, the cost of control grows with better regulation performances: the control valve has to move more when trying to compensate for faster disturbances. The new algorithms perform well also in the rejection of a demand step variation, with satisfying settling times and no or very little oscillations in the response, as discussed in § 6 (fire hydrant opening simulations).

Control Algorithm	*Displacement Instants* [%]	$\sum\|\Delta\alpha\|$ [−]	$Mean\|e(k)\|$ [m]
PI	100	33.5	0.7
FPI with SP	100	11.4	0.74
ILQG with SP	100	20	0.7
P on ξ	2	3.37	1.06

Table 11: Case Study B: performance comparison of algorithms tested on the WDN with Demand A.

Control Algorithm	*Displacement Instants* [%]	$\sum\|\Delta\alpha\|$ [−]	$Mean\|e(k)\|$ [m]
PI	98	22.9	0.55
FPI with SP	98	9.6	0.62
ILQG with SP	98	15	0.6
P on ξ	2.75	5.55	0.98

Table 12: Case Study B: performance comparison of algorithms tested on the WDN with Demand B.

The results for Case Study B are summarised in Tables 11 and 12. Recall that a single tuning of the control algorithm was performed to cope with two different demand trends. Considerations about the percentage of displacement instants still hold. Note that a displacement instants of 98% is obtained with demand profile A because of saturation of the actuator (see Figure 22 as example). Again, all the new algorithms outperform the *P on ξ* benchmark. The best regulation performance is delivered by the *PI* algorithm. The power of pressure waves, which

were responsible for its bad performance in Case Study A, is now distributed over many harmonics. The PI could then be used with larger closed-loop bandwidths. Still, the cost of regulation is quite high when compared to $ILQG$ algorithm, which provides almost the same regulation performance with a significant reduction of control cost. Note that the results achieved with the $ILQG - SF$ algorithm are not reported because do not improve the one achieved without the shaping functions. The FPI algorithm instead further reduces the control cost, at the price of slightly worse regulation error.

8. Conclusion

Several model based control techniques for pressure regulation have been successfully implemented and tested with two different WDN case studies. A detailed numerical model is used for WDN simulations. The presented algorithms take into account the dynamic behaviour of the WDN around the nominal working point by means of a linear model, which is derived from simulations. All control algorithms improve the state of the art in terms of regulation error in presence of pulsed nodal demand. On average, the reduction in the regulation error adds up to about 40%. Pressure is quickly regulated to the setpoint even in presence of demand step variations. Note that these algorithms require very low computational power and can be easily implemented on low power devices. Their application in the field is viable in all the cases where the increase in control cost, which may cause the more rapid wearing of the control valve, is not a limiting factor. A requirement for the application of these algorithms operating with a sampling time of 1 s is the possibility to transfer continuously the pressure head signal from the remote note to the control valve site. This is easy in new WDNs, where wiring is already present alongside pipes. In old WDNs, where the absence of wiring alongside pipes makes wireless communication necessary, the use of control algorithms operating with longer sampling times may be preferable. The study of the presented algorithms with longer settling times is left as future work.

References

[1] M. Farley, S. Trow, Losses in water distribution networks, IWA publishing, 2003.

[2] J. Thornton, A. Lambert, Managing pressures to reduce new breaks, Water 21 (December 2006) (2006) 24–26.

[3] A. Lambert, M. Fantozzi, J. Thornton, Practical approaches to modeling leakage and pressure management in distribution systems–progress since 2005, in: Proceedings of the 12th Int. Conf. on Computing and Control for the Water Industry-CCWI2013, 2013.

[4] T. M. Walski, D. V. Chase, D. A. Savic, W. Grayman, S. Beckwith, E. Koelle, Advanced water distribution modeling and management, Haestad press, 2003.

[5] S. L. Prescott, B. Ulanicki, Improved control of pressure reducing valves in water distribution networks, Journal of hydraulic engineering 134 (1) (2008) 56–65.

[6] N. Fontana, M. Giugni, L. Glielmo, G. Marini, R. Zollo, Real-time control of pressure for leakage reduction in water distribution network: Field experiments, Journal of Water Resources Planning and Management 144 (3) (2017) 04017096.

[7] N. Fontana, M. Giugni, L. Glielmo, G. Marini, F. Verrilli, Real-time control of a prv in water distribution networks for pressure regulation: Theoretical framework and laboratory experiments, Journal of Water Resources Planning and Management 144 (1) (2017) 04017075.

[8] T. Janus, B. Ulanicki, Improving stability of electronically controlled pressure-reducing valves through gain compensation, Journal of Hydraulic Engineering 144 (8) (2018) 04018053.

[9] A. Campisano, E. Creaco, C. Modica, Rtc of valves for leakage reduction in water supply networks, Journal of Water Resources Planning and Management 136 (1) (2009) 138–141.

[10] A. Campisano, C. Modica, L. Vetrano, Calibration of proportional controllers for the rtc of pressures to reduce leakage in water distribution networks, Journal of Water Resources Planning and Management 138 (4) (2011) 377–384.

[11] A. Campisano, C. Modica, S. Reitano, R. Ugarelli, S. Bagherian, Field-oriented methodology for real-time pressure control to reduce leakage in water distribution networks, Journal of Water Resources Planning and Management 142 (12) (2016) 04016057.

[12] E. Creaco, M. Franchini, A new algorithm for real-time pressure control in water distribution networks, Water Science and Technology: Water Supply 13 (4) (2013) 875–882.

[13] E. Creaco, T. Walski, Economic analysis of pressure control for leakage and pipe burst reduction, Journal of Water Resources Planning and Management 143 (12) (2017) 04017074.

[14] G. Cembrano, G. Wells, J. Quevedo, R. Pérez, R. Argelaguet, Optimal control of a water distribution network in a supervisory control system, Control engineering practice 8 (10) (2000) 1177–1188.

[15] C. Ocampo-Martinez, V. Puig, G. Cembrano, J. Quevedo, Application of predictive control strategies to the management of complex networks in the urban water cycle [applications of control], IEEE Control Systems 33 (1) (2013) 15–41.

[16] C. Ocampo-Martinez, D. Barcelli, V. Puig, A. Bemporad, Hierarchical and decentralised model predictive control of drinking water networks: Application to barcelona case study, IET control theory & applications 6 (1) (2012) 62–71.

[17] J. Grosso, C. Ocampo-Martínez, V. Puig, B. Joseph, Chance-constrained model predictive control for drinking water networks, Journal of process control 24 (5) (2014) 504–516.

[18] J. M. Grosso, P. Velarde, C. Ocampo-Martinez, J. M. Maestre, V. Puig, Stochastic model predictive control approaches applied to drinking water networks, Optimal Control Applications and Methods 38 (4) (2017) 541–558.

[19] J. M. Grosso, J. M. Maestre, C. Ocampo-Martinez, V. Puig, On the assessment of tree-based and chance-constrained predictive control approaches applied to drinking water networks, IFAC Proceedings Volumes 47 (3) (2014) 6240 – 6245, 19th IFAC World Congress.

[20] R. Toro, C. Ocampo-Martínez, F. Logist, J. V. Impe, V. Puig, Tuning of predictive controllers for drinking water networked systems, IFAC Proceedings Volumes 44 (1) (2011) 14507 – 14512, 18th IFAC World Congress.

[21] E. Creaco, Exploring numerically the benefits of water discharge prediction for the remote rtc of wdns, Water 9 (12) (2017) 961.

[22] P. R. Page, A. M. Abu-Mahfouz, S. Yoyo, Parameter-less remote real-time control for the adjustment of pressure in water distribution systems, Journal of Water Resources Planning and Management 143 (9) (2017) 04017050.

[23] E. Creaco, A. Campisano, M. Franchini, C. Modica, Unsteady flow modeling of pressure real-time control in water distribution networks, Journal of Water Resources Planning and Management 143 (9) (2017) 04017056.

[24] B. Ulanicki, P. Skworcow, Why prvs tends to oscillate at low flows, Procedia Engineering 89 (2014) 378–385.

[25] T. Janus, B. Ulanicki, Hydraulic modelling for pressure reducing valve controller design addressing disturbance rejection and stability properties, Elsevier, 2017.

[26] J. Van Zyl, A. Cassa, Modeling elastically deforming leaks in water distribution pipes, Journal of Hydraulic Engineering 140 (2) (2013) 182–189.

[27] G. Pezzinga, Evaluation of unsteady flow resistances by quasi-2d or 1d models, Journal of Hydraulic Engineering 126 (10) (2000) 778–785.

[28] V. L. Streeter, E. B. Wylie, K. W. Bedford, Fluid mechanics, wcb (1998).

[29] C. Ciaponi, L. Franchioli, E. Murari, S. Papiri, Procedure for defining a pressure-outflow relationship regarding indoor demands in pressure-

727 driven analysis of water distribution networks, Water resources manage-
728 ment 29 (3) (2015) 817–832.
729 [30] L. Ljung, System identification toolbox: for use with MATLAB: user's
730 guide, Math Works, 1991.
731 [31] D. E. Seborg, D. A. Mellichamp, T. F. Edgar, F. J. Doyle III, Process
732 dynamics and control, John Wiley & Sons, 2010.
733 [32] L. Magni, R. Scattolini, Advanced and multivariable control, Pitagora,
734 2014.